A serendipity triangular patch for evaluating weakly singular boundary integrals

Yudong Zhong[a], Jianming Zhang[a,b], Yunqiao Dong[a], Yuan Li[a], Weicheng Lin[a] and Jinyuan Tang[b]

[a]State Key Laboratory of Advanced Design and Manufacturing for Vehicle Body, Hunan University, Changsha 410082, China

[b]State Key Laboratory of High Performance Complex Manufacturing, Central South University, Changsha 410083, China

*Correspondence to: Jianming Zhang

College of Mechanical and Vehicle Engineering, Hunan University, Changsha 410082, China

Telephone: +86-731-88823061

E-mail: zhangjm@hnu.edu.cn

Abstract: Element subdivision is the most widely used method for the numerical evaluation of weakly singular integrals in three-dimensional boundary element analyses. In the traditional subdivision method, the sub-elements, which are called patches in this paper, are obtained by simply connecting the singular point with each vertex of the element. Patches with large angles at the source point may be produced and thus, a large number of Gaussian quadrature points are needed to achieve acceptable accuracy. In this paper, a serendipity triangular patch with four-node is presented to solve the problem. Case studies have been made to investigate the effect of the location of the middle node of the serendipity patch on accuracy, and an optimal location is determined. Moreover, theoretical analysis validating the optimal location is also given with a new form of polar coordinate transformation. Numerical examples are presented to compare the new patch with the conventional linear patch with respect to both accuracy and efficiency. In all cases, the results are encouraging.

Keywords: *Boundary element, weakly singular integral, serendipity triangular patch, Gaussian quadrature, element subdivision method.*

1. Introduction

Accurate and efficient evaluation of weakly singular integrals arising in the boundary integral equations (BIEs) is of crucial importance for successful implementation of the boundary element method (BEM) [1-6]. Much effort has been made to remove the weakly singular integrals

appearing in BIEs. And there are many ways of evaluating singular integrals mentioned in the boundary element literature. These approaches include integral simplification [7], element subdivision [8] and coordinate transformation [9], with each method having its advantages and disadvantages. Element subdivision is one of the most widely used methods for the numerical evaluation of weakly singular integrals. Many different element subdivision methods have been proposed. Klees has proposed a subdivision method and the sub-elements which are also called patches are obtained by simply connecting the singular point with each vertex of the element [8]. Zhang *el al* have used the subdivision method coupled with a new coordinate transformation which is denoted as (α-β) transformation to remove singularities [10] and further developed an adaptive element subdivision method named Quad-tree subdivision [11]. Obviously, all the above element subdivision methods may produce patches in "bad" shapes. Moreover, polar coordinate transformation is a powerful and useful tool to evaluate weakly singular integral in boundary element. It converses the surface integral into a double integral in radial and angular directions. Many works have been done on dealing with the singularity in the radial direction; however, numerical integration on the angular direction still deserves more attention. In fact, after singularity cancelation or subtraction, although the integrand may behave very well in the radial direction, its behavior in the angular direction would be much worst, so too many quadrature points are needed. Especially when the source point lies close to the boundary of the element, one can clearly observe near singularity of the integrand in the angular direction. Similar problems have been considered in work about the nearly singular BEM integrals. Effective methods along this line are the subdivision method [12], the Hayami transformation [13], the sigmoidal transformation [14], the conformal transformation [15], the variable transformation [16], etc.

In this paper, Sphere subdivision method proposed by Zhang is used [17], and based on this method; first a serendipity triangular patch which is obtained by the element subdivision is introduced to overcome the problem of the integral in the angular direction. One edge of the patch is replaced by quadratic curve, the distance between the middle node of the quadratic curve and the source point is equal to the length of radius of the sphere which is centered at the source point. Then the polar coordinate system with new form is used in this patch. This system is very similar to the conventional polar system, but its implementation is simpler than the conventional polar system and also performs efficiently. Using the coordinate transformation, the integrals with

weakly singularities can be accurately calculated. Furthermore, in order to investigate the effect of the location of the middle node on the computational accuracy, its location is changed along the direction of the source point to the middle node step by step. Through theoretical analysis and numerical experiment, the location with the highest accuracy has been found in this paper. With our method, the weakly singular boundary integrals in the regular or irregular elements can be accurately and effectively calculated. And our method can be also applied to the patch with large angles at the source point. Numerical examples are presented to validate the proposed method. Results demonstrate the accuracy and efficiency of our method.

This paper is organized as follows. Detailed description of the serendipity triangular patch and the coordinate system with new form are described in Section 2. In Section 3, the effect of the middle node's location in the serendipity triangular patch is introduced. Numerical examples are given in Section 4. The paper ends with conclusions in Section 5.

2. Four-nodes serendipity triangular patch

To achieve the best balance between accuracy and efficiency, it is desirable that subdivided patches closer to the source point have relatively smaller sizes. To guarantee this, we use a sequence of spheres centered at the source point with decreasing radius to cut the element, recursively. And a serendipity triangular patch with four-nodes is obtained through the element subdivision.

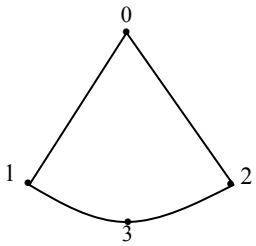

Figure 1. Four-nodes serendipity triangular patch.

The serendipity triangular patch is as shown in Fig. 1, the following symbols are defined:

0——the source point;

3——the middle node;

0, 1, 2, 3——serendipity patch node;

In the serendipity patch, the distance between point 0 and point 3 is equal to the length of radius of the sphere which is centered at the source point. And the length of radius we can

obtain in [17]. For the patches containing source point, the coordinate transformation is used to eliminate the singularities.

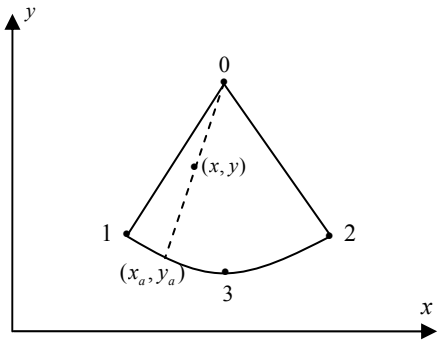

Figure 2. The coordinate transformation of serendipity triangular patch.

Considering the weakly singular integral over a patch as shown in Fig. 2, the following boundary integral can be represented as

$$I(y)=\int_s \frac{f(y,r)}{r}\phi(x)dS \tag{1}$$

where y and x are referred to as the source point and the field point, respectively, r is the distance between y and x, f is a well-behaved function, and $\phi(x)$ is a shape function.

For this patch, to construct the local (ρ, θ) system, the following mapping is used:

$$\begin{cases} x_a = N_0 x_1 + N_1 x_2 + N_2 x_3 \\ y_a = N_0 y_1 + N_1 y_2 + N_2 y_3 \end{cases} \tag{2a}$$

In the Eq. (2a), N_0, N_1 and N_2 are the shape functions of the quadratic curve.

$$\begin{aligned} N_0 &= \frac{1}{2}\theta(\theta-1) \\ N_2 &= (1+\theta)(1-\theta) \\ N_1 &= \frac{1}{2}\theta(\theta+1) \end{aligned} \tag{2b}$$

$$\begin{cases} x = x_0 + (x_a - x_0)\rho \\ y = y_0 + (y_a - y_0)\rho \end{cases} \quad \rho \in [0,1], \theta \in [-1,1] \tag{2c}$$

Combining Eq. (2a), 2(b) and (2c), the coordinate transformation can be written as:

$$\begin{cases} x = x_0 + \left([N_0 x_1 + N_2 x_3 + N_1 x_2] - x_0\right)\rho \\ y = y_0 + \left([N_0 y_1 + N_2 y_3 + N_1 y_2] - y_0\right)\rho \end{cases} \tag{3}$$

Then the integral I can be written as

$$I=\int_{-1}^{1}\int_{0}^{1}\frac{f(y,r)}{r}Jb(\rho,\theta)\phi d\rho d\theta \tag{4}$$

Where $Jb(\rho,\theta)$ is the Jacobian of the transformation from the x-y system to the ρ-θ system,

$$Jb(\rho,\theta)=\rho\left[(x_a-x_0)\frac{\partial y_a}{\partial\theta}-(y_a-y_0)\frac{\partial x_a}{\partial\theta}\right] \tag{5}$$

From Eq. (2) to Eq. (5), it can be noted that the new coordinate system is much simpler to implement than the conventional polar coordinate system [9]. This is due to the fact that ρ and θ are constrained to the interval [0, 1] and [-1, 1] in this triangle, thus there is no need to calculate their spans. So our method may be computationally more efficient.

3. The effect of the middle node's location

3.1 Changing the middle node's location

In this section, we will investigate the effect of the middle node's location on the computational accuracy. As shown in Fig. 3, its location is changed along the direction of the source point to the middle node by using the Eq. (6).

$$\begin{aligned} x_3 &= x_q + (x_p - x_q)t \\ y_3 &= y_q + (y_p - y_q)t \\ x_q &= \frac{x_1 + x_2}{2} \qquad y_q = \frac{y_1 + y_2}{2} \end{aligned} \tag{6}$$

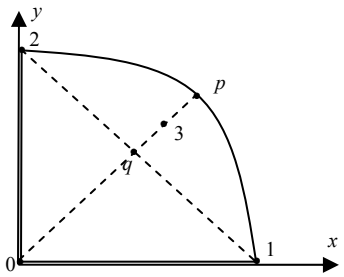

Figure 3. The location of the middle node in the serendipity triangular patch.

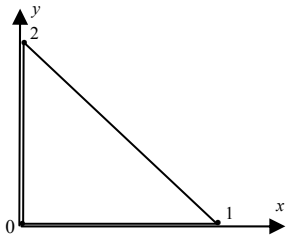

Figure 4. Conventional linear triangle patch.

As both *Jb* and *r* have ρ so we can turn it off. The plot of the function $f(\theta)=Jb/r$ on the conventional triangle patch and the serendipity triangle patch is made by MATLAB. As shown in Fig. 5, the plots of $f(\theta)$ have expressed when *t* takes different values, respectively. As we can see when *t* move close to 0.5, the plots of the function become gentler and gentler. And when *t* is equal to 0.5, the plot becomes a horizontal line. So when *t* changes from 0.1 to 1.0, the plots of the function on the serendipity triangular patch is gentler than that on the conventional linear triangle patch (t=0). Thus compared with conventional triangle patch, high accuracy results can be

obtained with less Gaussian quadrature points by using the proposed serendipity triangular patch.

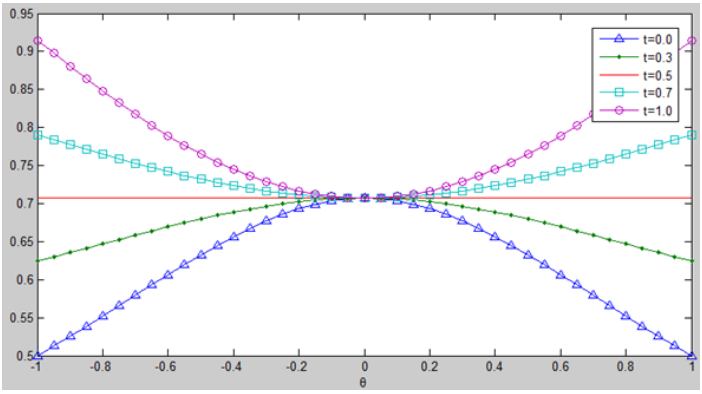

Figure 5. The plots of function *Jb/r*.

3.2 The triangle patch with large angles

The element subdivision used in this paper is called sphere subdivision method [17]. An element is subdivided into a number of patches through a sequence of spheres with decreasing radius, the obtained patches are automatically refined as they approaching the source point and the patches also have the same aspect ratio. The patches with large angles at the source point may be produced through the element subdivision. And there are some difficulties on the integrals of the angular direction in these patches.

Using Eq. (3) and Eq. (5), the Eq. (7) can be obtained [18]. And using Eq. (7b), we can obtain the derivative of g(θ) as shown in Eq. (7c).

$$f(\theta)=\frac{Jb(\rho,\theta)}{r(\rho,\theta)}=\frac{\rho\left[(x_a-x_0)\frac{\partial y_a}{\partial\theta}-(y_a-y_0)\frac{\partial x_a}{\partial\theta}\right]}{\rho\sqrt{(x_a-x_0)^2+(y_a-y_0)^2}}=\frac{g(\theta)}{r_1} \tag{7a}$$

$$g(\theta)=(x_a-x_0)\frac{\partial y_a}{\partial\theta}-(y_a-y_0)\frac{\partial x_a}{\partial\theta} \tag{7b}$$

$$\begin{aligned} g'(\theta)&=(x_a-x_0)\frac{\partial^2 y_a}{\partial\theta^2}-(y_a-y_0)\frac{\partial^2 x_a}{\partial\theta^2}+\frac{\partial x_a}{\partial\theta}\frac{\partial y_a}{\partial\theta}-\frac{\partial x_a}{\partial\theta}\frac{\partial y_a}{\partial\theta} \\ &=(x_a-x_0)(y_1+y_2-2y_3)-(y_a-y_0)(x_1+x_2-2x_3) \end{aligned} \tag{7c}$$

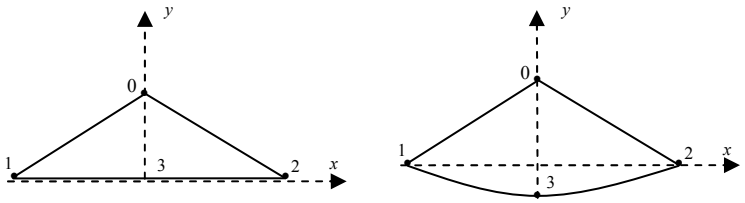

(a) (b)

Figure 6. (a) Conventional linear triangle patch; (b) serendipity triangular patch.

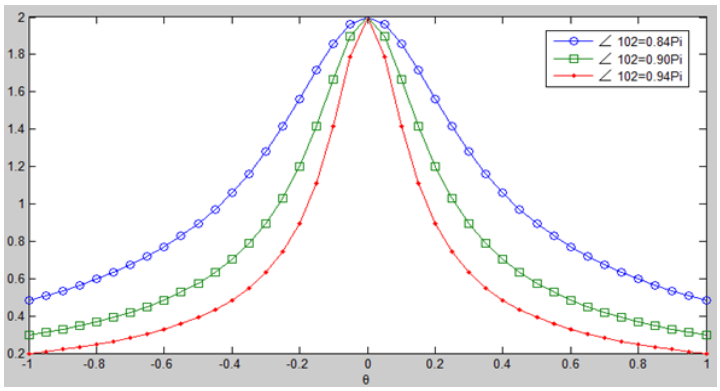

Figure 7. The plots of function *Jb/r*.

The conventional linear triangle patch as shown in Fig. 6(a), when the angle $\angle 102$ takes different values, the plots of the Eq. (7a) have been made by MATLAB. And r_1 is the distance between the source point to the point of the edge 12. As shown in Fig. 7, when the angle increase gradually, the plots of function *f(θ)=Jb(ρ,θ)/r* are becoming steeper and steeper. The reason is as follows: the point 3 is the midpoint of the point 1 and 2, from Eq. (7b) to Eq. (7c) it can be noted that *g(θ)* is a constant. Therefore, when the angle $\angle 102$ is gradually increase, the change of r_1 will become more and more acutely. When r_1 is close to zero, the near singularity in *f(θ)* can be clearly seen from Fig. (7).

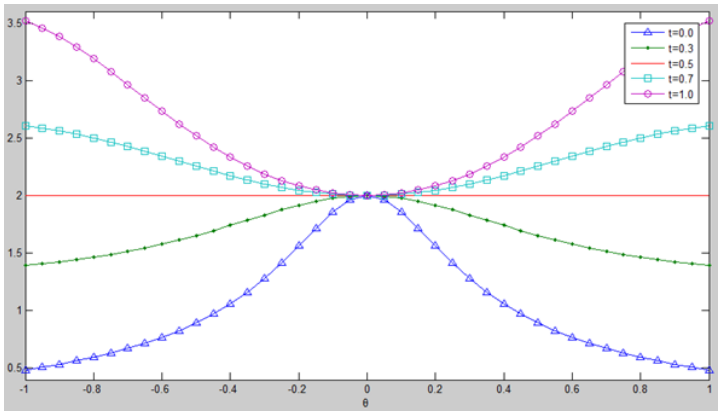

Figure 8. The plots of function *Jb/r*.

If the serendipity triangular patch as shown in Fig. 6(b) is used to substitute the conventional linear triangular patch, the variety of r_1 becomes less evident and the function of *g(θ)* isn't a constant. When the angle $\angle 102$ is equal to 0.84π, the plots of the function *f(θ)=Jb(ρ, θ)/r* are

shown in Fig. 8. It can be clearly seen that the curve in the plot become gentler and gentler when t is changed close to 0.5. So when evaluating the function $f(\theta)$, more accurate results can be obtained by using the serendipity triangular patch.

3.3 The best location of the middle node

In this section, the best location of the middle node is found when t is equal to 0.5. The theoretical analysis is given to verify that. And more details of the theoretical analysis are as follows.

The Eq. (3) can be written as the form of the Eq. (8).

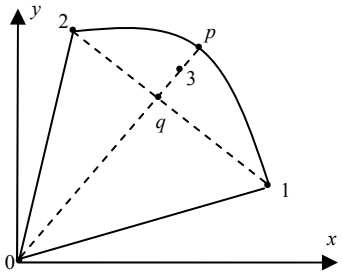

Figure 9. The location of the middle node in the serendipity triangular patch.

$$
\begin{aligned}
&x = x_0 + (a_1\theta^2 + b_1\theta + c_1)\rho \\
&y = y_0 + (a_2\theta^2 + b_2\theta + c_2)\rho \\
&\frac{\partial x}{\partial \rho} = a_1\theta^2 + b_1\theta + c_1 \qquad \frac{\partial x}{\partial \theta} = (2a_1\theta + b_1)\rho \\
&\frac{\partial y}{\partial \rho} = a_2\theta^2 + b_2\theta + c_2 \qquad \frac{\partial y}{\partial \theta} = (2a_2\theta + b_2)\rho
\end{aligned} \tag{8a}
$$

$$
\begin{aligned}
&a_1 = 0.5x_1 + 0.5x_2 - x_3 \qquad a_2 = 0.5y_1 + 0.5y_2 - y_3 \\
&b_1 = -0.5x_1 + 0.5x_2 \qquad b_2 = -0.5y_1 + 0.5y_2 \\
&c_1 = x_3 - x_0 \qquad c_2 = y_3 - y_0
\end{aligned} \tag{8b}
$$

From the element subdivision, we can obtain that the line segment 03 is perpendicular to line segment 12, and the edges 02, 01, and 0p have the same length R obtained by element subdivision [17]. In order to conveniently calculate the coordinate of the point p, the source point is placed in (0, 0). The coordinate of the point p and the point 3 can be obtained by Eq. (9) and as shown in Eq. (10).

$$
\begin{aligned}
&(x_p - x_0)(x_2 - x_1) + (y_p - y_0)(y_2 - y_1) = 0 \\
&(x_p - x_0)^2 + (y_p - y_0)^2 = (x_1 - x_0)^2 + (y_1 - y_0)^2 = (x_2 - x_0)^2 + (y_2 - y_0)^2 = R^2
\end{aligned} \tag{9}
$$

$$x_p = x_0 + \frac{y_2 - y_1}{x_1 - x_2}\frac{R}{\sqrt{1+(\frac{y_2 - y_1}{x_1 - x_2})^2}} \qquad y_p = y_0 + \frac{R}{\sqrt{1+(\frac{y_2 - y_1}{x_1 - x_2})^2}} \tag{10a}$$

$$\begin{aligned} x_3 &= \frac{x_1 + x_2}{2} + (x_p - \frac{x_1 + x_2}{2})t \\ y_3 &= \frac{y_1 + y_2}{2} + (y_p - \frac{y_1 + y_2}{2})t \end{aligned} \tag{10b}$$

$$\begin{aligned} r^2 &= (x - x_0)^2 + (y - y_0)^2 = x^2 + y^2 \\ &= (a_1^2 + a_2^2)\theta^4 + (2a_1b_1 + 2a_2b_2)\theta^3 + (2a_1c_1 + 2a_2c_2 + b_1^2 + b_2^2)\theta^2 \\ &+ (2b_1c_1 + 2b_2c_2)\theta + c_1^2 + c_2^2 \\ Jb^2 &= (\frac{\partial x}{\partial \rho}\frac{\partial y}{\partial \theta} - \frac{\partial y}{\partial \rho}\frac{\partial x}{\partial \theta})^2 \\ &= \left\{ \begin{array}{l} (a_2b_1 - a_1b_2)^2\theta^4 + (2a_2b_1 - 2a_1b_2)(2a_2c_1 - 2a_1c_2)\theta^3 \\ \quad + [2(a_2b_1 - a_1b_2)(c_1b_2 - c_2b_1) + (2a_2c_1 - 2a_1c_2)^2]\theta^2 \\ \quad + 2(2a_2c_1 - 2a_1c_2)(c_1b_2 - c_2b_1)\theta + (c_1b_2 - c_2b_1)^2 \end{array} \right\} \rho^2 \end{aligned} \tag{11}$$

Using Eq. (8a) and Eq. (8b), the Eq. (11) can be obtained. As the line segment 12 is perpendicular to the line segment 0*p* and the slope of the line *pq* is equal to that of the line 03. The Eq. (12) can be obtained.

$$\begin{aligned} 2a_1b_1 + 2a_2b_2 &= 0 \\ 2b_1c_1 + 2b_2c_2 &= 0 \\ 2a_2c_1 - 2a_1c_2 &= 0 \end{aligned} \tag{12}$$

Using Eq. (12), Eq. (11) can be written as:

$$\begin{aligned} Jb^2 &= [(a_2b_1 - a_1b_2)^2\theta^4 + 2(a_2b_1 - a_1b_2)(c_1b_2 - c_2b_1)\theta^2 + (c_1b_2 - c_2b_1)^2]\rho^2 \\ r^2 &= [(a_1^2 + a_2^2)\theta^4 + (2a_1c_1 + 2a_2c_2 + b_1^2 + b_2^2)\theta^2 + c_1^2 + c_2^2]\rho^2 \end{aligned}$$

And Eq. (11) can be further written as [18]:

$$\begin{aligned} Jb^2 &= (a_2b_1 - a_1b_2)^2\theta^4 + 2(a_2b_1 - a_1b_2)(c_1b_2 - c_2b_1)\theta^2 + (c_1b_2 - c_2b_1)^2 \\ &= \alpha^2(a_2b_1 - a_1b_2)^2[\theta^2 + \frac{c_1b_2 - c_2b_1}{a_2b_1 - a_1b_2}]^2 \\ r^2 &= \alpha^2[(a_1^2 + a_2^2)\theta^4 + (2a_1c_1 + 2a_2c_2 + b_1^2 + b_2^2)\theta^2 + c_1^2 + c_2^2] \\ &= \alpha^2\left\{(a_1^2 + a_2^2)[\theta^2 + \frac{(2a_1c_1 + 2a_2c_2 + b_1^2 + b_2^2)}{2(a_1^2 + a_2^2)}]^2 + (c_1^2 + c_2^2) - \frac{(2a_1c_1 + 2a_2c_2 + b_1^2 + b_2^2)^2}{4(a_1^2 + a_2^2)}\right\} \end{aligned} \tag{13}$$

$$M = 4(c_1^2 + c_2^2)(a_1^2 + a_2^2) - (2a_1c_1 + 2a_2c_2 + b_1^2 + b_2^2)^2 \tag{14}$$

$$x_1^2 = R - y_1^2 \qquad x_2^2 = R - y_2^2 \tag{15}$$

Substitute the parameter *a1*, *a2*, *b1*, *b2*, *c1*, *c2* and Eq. (15) into Eq. (14) and Eq. (16), respectively. Calculate it in MAPLE 15 when *t* is equal to 0.5, *M*=0 and *N*=0 can be easily obtained. So *t*=0.5 is a common root of the equation *M*(*t*)=0 and *N*(*t*)=0.

$$N = 2(c_1 b_2 - c_2 b_1)(a_1^2 + a_2^2) - (2a_1 c_1 + 2a_2 c_2 + b_1^2 + b_2^2)(a_2 b_1 - a_1 b_2) \tag{16}$$

That is to say, when t is equal to 0.5, the Eq. (17) is workable and the ratio of $Jb(\rho,\theta)/r$ has nothing to do with ρ and θ. And the ratio A can be expressed as follows in Eq. (18).

$$\begin{cases} \dfrac{c_1 b_2 - c_2 b_1}{a_2 b_1 - a_1 b_2} = \dfrac{(2a_1 c_1 + 2a_2 c_2 + b_1^2 + b_2^2)}{2(a_1^2 + a_2^2)} \\ (c_1^2 + c_2^2) - \dfrac{(2a_1 c_1 + 2a_2 c_2 + b_1^2 + b_2^2)^2}{4(a_1^2 + a_2^2)} = 0 \end{cases} \tag{17}$$

$$A = \frac{(a_2 b_1 - a_1 b_2)^2}{(a_1^2 + a_2^2)} \tag{18}$$

With the detailed description above, it can be clearly seen that our method has obvious advantages over conventional method. Firstly, the plots of the integrand of the angular direction become quite gentle. Secondly, as the patches obtained are automatically refined as they approaching the source point, Gaussian sample points are set denser around the source point to get an accurate enough result. Away from the source point, Gaussian sample points are sparsely distributed, much fewer but enough to guarantee an accurate result, so a large number of unnecessary Gaussian sample points are avoided. In a word, with the serendipity triangular patch coupled with the coordinate transformation, the weakly singular integrals can be solved with higher accuracy and less computational cost.

4. Numerical examples

To evaluate the effectiveness and accuracy of our method, in this section, several comparisons are made between our method and the conventional method for planar element and curved surface element. For the purpose of error estimation, relative error is defined as follows:

$$\text{Relative Error} = \left| \frac{I_n - I_e}{I_e} \right| \tag{19}$$

Where I_n is the numerical solution, and I_e is the exact solution of the integral.

We consider the numerical evaluation of the integral

$$I = \int_\Gamma \frac{1}{r} \phi d\Gamma \tag{20}$$

In Eq. (20), where Γ is an arbitrary boundary element and ϕ is a shape function of the element. And in all the numerical examples, the above coordinate transformation is used to remove singularities in the patches which contain the source point, while the remaining regular quadrilateral and triangular patches are respectively evaluated by the standard Gaussian quadrature. The number of the Gaussian points m is determined by [19-21].

$$m = \sqrt{\frac{2}{3} p + \frac{2}{5}} \left[-\ln\left(\frac{e}{2}\right) \Big/ 10 \right] \left[\left(\frac{8L}{3R}\right)^{\frac{3}{4}} + 1 \right] \tag{21}$$

Where p represents the order of the singularity (p=1,2,3). e denotes the error tolerance. L is the length of patch in integral direction. And R is the minimum distance from the source point to the boundary element.

4.1 Examples of serendipity triangle patch

In this example, we study the influence of the middle node's location on the computational accuracy in our method when the source point is fixed. As shown in Fig.11, three vertexes of the patch located at (0, 1, 0), (-2, 0, 0) and (2, 0, 0), respectively. In each case, the source point is fixed at (0, 1, 0), and the middle node 3 is determined by an offset parameter $t, 0 \le t \le 1$, using the following equation :

$$x_3 = \frac{x_1 + x_2}{2} + (x_p - \frac{x_1 + x_2}{2})t$$
$$y_3 = \frac{y_1 + y_2}{2} + (y_p - \frac{y_1 + y_2}{2})t \qquad (10b)$$

$$x_p = 0.0 \qquad y_p = 1.0 - \frac{\sqrt{5}}{\sqrt{1 + (\frac{y_2 - y_1}{x_1 - x_2})^2}} = 1.0 - \sqrt{5}$$

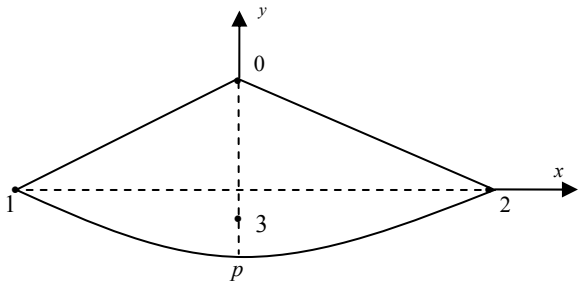

Figure 10. The location of the middle point of the serendipity triangular patch.

Table 1: Gaussian points number used by linear and serendipity patch in case of equivalent accuracy.

	Gaussian points number			Relative Error
	(angular direction)	(radius direction)	total	
Conventional method (t=0.0)	14	5	70	7.14e-007
Our method (t=0.3)	10	5	50	2.34e-007
Our method (t=0.5)	2	5	10	3.33e-016
Our method (t=0.7)	7	5	35	2.86e-008
Our method (t=1.0)	7	5	35	9.97e-007

The accuracy obtained by both our method and the conventional method and the number of the Gaussian sample points used are listed in Table 1 and Table 2. It is seen that to obtain the same

level of accuracy, our method needs much fewer sample points, and thus, considerably increases the computational efficiency. And as illustrated in Table 1 and Table 2, from the numerical solutions obtained we can find that when t = 0.5, we can obtain the highest accuracy with the fewest Gaussian sample points.

Table 2: accuracy obtained by linear and serendipity patch in case of equivalent Gaussian sample points.

	Gaussian points number			Relative Error
	(angular direction)	(radius direction)	total	
Conventional method (t=0.0)	7	5	35	8.43e-004
Our method (t=0.3)	7	5	35	2.31e-005
Our method (t=0.5)	7	5	35	3.33e-016
Our method (t=0.7)	7	5	35	2.86e-008
Our method (t=1.0)	7	5	35	9.97e-007

4.2 Examples of triangle element with large-angle

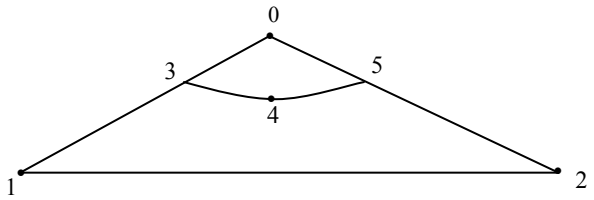

Figure 11. Subdivisions of planar triangular element with our method.

In this part, we study the numerical evaluation of the triangle element in our method when t = 0.5. Three vertexes of the element are located at (0, 1, 0), (-4, 0, 0) and (4, 0, 0), respectively. And the source point is fixed at (0, 1, 0). Through adaptive element subdivision [17], the element is subdivided two patches as shown in Fig. 11. And the angle at the source point is approximate equal to 0.84π. The coordinate of point 3, 4 and 5 can be calculated by using Eq. (10b).

Table 3: Numerical evaluation for planar triangular element.

	Gaussian points number	Relative Error	Gaussian points number	Relative Error
Conventional method	55	1.68e-003	130	9.05e-007
Our method (t=0.5)	54	8.11e-006	87	5.60e-007

The accuracy obtained by both our method and the conventional method and the number of

the Gaussian sample points used are listed in Table 3. It can be seen that to obtain the same level of accuracy, our method needs much fewer sample points, and thus, considerably increases the computational efficiency.

4.3 Examples of planar element

In this example, we study the numerical evaluation of the planar quadrilateral element and slender quadrilateral element in our method when t = 0.5. The vertexes of the planar element are located at (1, 1, 0), (-1, 1, 0), (-1, -1, 0), (1, -1, 0) and that of the slender element are (5, 1, 0), (-5, 1, 0), (-5, -1, 0), (5, -1, 0), respectively. And the source point is fixed at (0, -0.9, 0). As shown in Fig. 12 and Fig. 13, the source points are very close to the edge. Through adaptive element subdivision [17], the element is subdivided into a few patches as shown in Fig. 12(b) and Fig. 13(b).

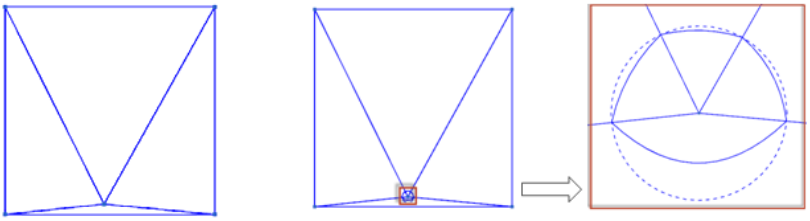

(a) the conventional method (b) Our method

Figure 12. Subdivisions of planar quadrilateral element with our method.

Table 4: Numerical evaluation for planar quadrilateral element.

	Gaussian points number	Relative Error	Gaussian points number	Relative Error
Conventional method	672	3.01e-004	1664	7.79e-007
Our method (t=0.5)	652	3.95e-006	872	4.81-007

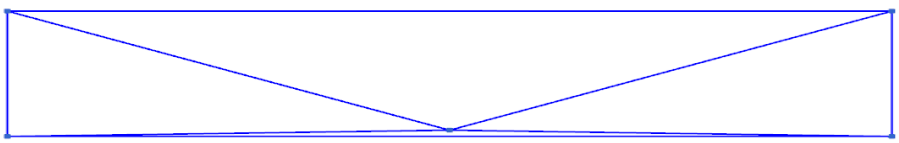

(a) the conventional method

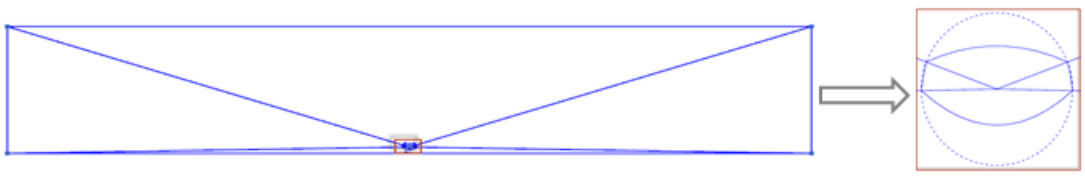

(b) Our method

Figure 13. Subdivisions of slender quadrilateral element with our method.

Table 5: Numerical evaluation for slender quadrilateral element.

	Gaussian points number	Relative Error	Gaussian points number	Relative Error
Conventional method	1600	9.30e-004	9600	9.41e-007
Our method (t=0.5)	1592	1.40e-005	3408	4.81-007

The accuracy obtained by both our method and the conventional method and the number of the Gaussian sample points used are listed in Table 4 and Table 5. It is seen that when the number of Gaussian sample points used is the same, the accuracy obtained by our method is higher than that by the conventional method. And to obtain the same level of accuracy, our method needs much fewer sample points. The effectiveness and accuracy of our method are demonstrated again.

4.4 Examples of curved surface element

In this part, we study the numerical evaluation of the curved quadrilateral element in our method when t = 0.5. The vertexes of the element are located at (1, 1, 1), (-1, 1, 0), (-1, -1, 1), (1, -1, 0) and the mid-nodes are located at (0, 1, 0.7), (-1, 0, 0.6), (0, -1, 0.5) and (1, 0, 0.7). And the source point is fixed at (0, -0.9, 0.538). And the mapped element as shown in Fig. 14, the source points are very close to the edge. As element subdivision technique we used is subdivided at the local coordinate system, so through adaptive element subdivision [17], the element is subdivided into a few patches as shown in Fig. 14(b).

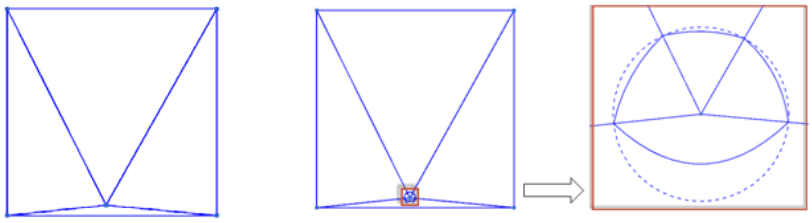

(a) the conventional method (b) Our method

Figure 14. Subdivisions of curved quadrilateral element with our method.

Table 6: Numerical evaluation for curved quadrilateral element.

	Gaussian points number	Relative Error	Gaussian points number	Relative Error
Conventional method	640	2.53e-004	2208	2.22e-007
Our method (t=0.5)	612	1.12e-005	916	3.03-007

The accuracy obtained by both our method and the conventional method and the number of the Gaussian sample points used are listed in Table 6. It is seen that when the number of Gaussian sample points used is the same, the accuracy obtained by our method is higher than that by the conventional method. And to obtain the same level of accuracy, our method needs much fewer sample points. The effectiveness and accuracy of our method are demonstrated again.

5. Conclusions

In this paper, a serendipity triangle patch with four-node is introduced for calculating the singular integrals in the BIE. By theoretical analysis and numerical experiment, the optimal location of the middle node of the serendipity patch has been found for the highest accuracy and efficiency. From the numerical examples, it has been demonstrated that our method can achieve much better accuracy than the conventional method with equivalent number of Gaussian sample points. On the other hand, to obtain the same level of accuracy, our method requires much fewer sample points, and thus, considerably increases the computational efficiency. Extending our method to compute curved surface element and 3D nearly singular integral is straightforward and ongoing.

Acknowledgement

This research is supported by National Science Foundation of China (Grant No.11172098 and No. 11472102) , and in part by Open Research Fund of Key Laboratory of High Performance Complex Manufacturing, Central South University (Grant No. Kfkt2013-05).

References

[1] Zhang JM, Tanaka M, Matsumoto T. Meshless analysis of potential problems in three dimensions with the hybrid boundary node method. Int J Numer Meth Eng 2004; 59(9): 1147-1166.

[2] Xie GZ, Zhou FL, Zhang JM, Zheng XS, Huang C. New variable transformations for evaluating nearly singular integrals in 3D boundary element method. Eng Anal Bound Elem 2013; 37(9): 1169-1178.

[3] Ma H, Kamiya N. Distance transformation for the numerical evaluation of near singular boundary integrals with various kernels in boundary element method. Eng Anal Bound Elem 2002; 26(4): 329-339.

[4] Gao XW, Yang K, Wang J. An adaptive element subdivision technique for evaluation of various 2D singular boundary integrals. Eng Anal Bound Elem 2008; 32(8): 692-696.

[5] Niu ZR, Wendland WL, Wang XX, Zhou HL. A sim-analytic algorithm for the evaluation of the nearly singular integrals in three-dimensional boundary element methods. Comput Methods Appl Mech Eng 2005, 31: 949–64.

[6] Johnston P R. Application of sigmoidal transformations to weakly singular and near -

singular boundary element integrals[J]. International journal for numerical methods in engineering 1999, 45(10): 1333-1348.

[7] Kane JH. Boundary Element Analysis in Engineering Continuum Mechanics. Prentice-Hall: Englewood Cliffs, NJ, 1994.

[8] Klees R. Numerical calculation of weakly singular surface integrals. J Geodesy 1996; 70(11): 781-797.

[9] Telles JCF. A self-adaptive co-ordinate transformation for efficient numerical evaluation of general boundary element integrals. International Journal for Numerical Methods in Engineering 1987; 24: 959-973.

[10]Zhang JM, Qin XY, Han X, Li GY. A boundary face method for potential problems in three dimensions. Int J Numer Meth Eng 2009; 80(3): 320-337.

[11]Tanaka M, Zhang JM, Matsumoto T. Boundary-type meshless solution of potential problems: comparison between singular and regular formulations in hybrid BNM Transactions of JASCOME, Journal of Boundary Element Methods 2003; Vol.20, pp.21-26.

[12] Scuderi L.On the computation of nearly singular integrals in 3D BEM collocation. Int J Numer Methods Eng 2008; 74: 1733–1770.

[13] Hayami K. Variable transformations for nearly singular integrals in the boundary element method[J]. Publications of the Research Institute for Mathematical Sciences 2005; 41(4): 821-842.

[14] Johnston BM, Johnston PR, Elliott D. A new method for the numerical evaluation of nearly singular integrals on triangular elements in the 3D boundary element method. J Comput Appl Math 2013; 245: 148–161.

[15]Liu Y J, Zhang D, Rizzo F J. Nearly singular and hyper-singular integrals in the boundary element method[J]. Boundary Elements XV, 1993, 1: 453-468.

[16]Guizhong Xie, Fenglin Zhou, Jianming Zhang, Xingshuai Zheng and Cheng Huang. New variable transformations for evaluating nearly singular integrals in 3D boundary element method. Engineering Analysis with Boundary Elements, 2013; 37: 1169-1178.

[17]Jianming Zhang, Chenjun Lu and Xiuxiu Zhang. An adaptive element subdivision method for evaluation of weakly singular integrals in 3D BEM. Engineering Analysis with Boundary Elements 2015; 51: 213-219.

[18]Gao X W, Feng W Z, Yang K, et al. Projection plane method for evaluation of arbitrary high order singular boundary integrals. Engineering Analysis with Boundary Elements, 2015; 50: 265-274.

[19]Gao XW, Davies T G. Adaptive integration in elasto–plastic boundary element analysis.

Journal of the Chinese institute of engineers 2000; 23(3): 349-356.

[20] Bu S, Davies TG. Effective evaluation of non-singular integrals in 3D BEM. Advances in Engineering Software 1995; 23(2): 121-128.

[21] Lachat JC, Watson JO. Effective numerical treatment of boundary integral equations: A formulation for three-dimensional elastostatics. International Journal for Numerical Methods in Engineering 1976; 10(5): 991-1005.